Protein Structure and Folding:

Structural Basis for Antifreeze Activity of Ice-binding Protein from Arctic Yeast

Jun Hyuck Lee, Ae Kyung Park, Hackwon Do, Kyoung Sun Park, Sang Hyun Moh, Young Min Chi and Hak Jun Kim

J. Biol. Chem. 2012, 287:11460-11468.
doi: 10.1074/jbc.M111.331835 originally published online February 2, 2012

THE JOURNAL OF BIOLOGICAL CHEMISTRY VOL. 287, NO. 14, pp. 11460–11468, March 30, 2012

Structural Basis for Antifreeze Activity of Ice-binding Protein from Arctic Yeast*[S]

Received for publication, December 8, 2011, and in revised form, January 24, 2012 Published, JBC Papers in Press, February 2, 2012, DOI 10.1074/jbc.M111.331835

Jun Hyuck Lee[‡§1], Ae Kyung Park[¶1], Hackwon Do[‡§], Kyoung Sun Park[‡§], Sang Hyun Moh[‖], Young Min Chi[¶], and Hak Jun Kim[‡§2]

From the [‡]Division of Polar Life Sciences, Korea Polar Research Institute, Incheon 406-840, the [§]Department of Polar Sciences, University of Science and Technology, Incheon 406-840, the [¶]Division of Biotechnology, College of Life Sciences, Korea University, Seoul 136-713, and the [‖]Anti-Aging Research Institute of BIO-FD&C Co., Ltd., Incheon 405-849, Republic of Korea

Background: Ice-binding proteins improve the cold tolerance of cells by inhibiting ice growth and recrystallization.
Results: Crystal structure and mutagenesis data of LeIBP suggests the B face as an ice-binding site.
Conclusion: LeIBP structure adopts a β-helical fold and the aligned Thr/Ser/Ala residues are critical for ice binding.
Significance: LeIBP structure can serve as a structural model for a large number of IBPs.

Arctic yeast *Leucosporidium* sp. produces a glycosylated ice-binding protein (LeIBP) with a molecular mass of ~25 kDa, which can lower the freezing point below the melting point once it binds to ice. LeIBP is a member of a large class of ice-binding proteins, the structures of which are unknown. Here, we report the crystal structures of non-glycosylated LeIBP and glycosylated LeIBP at 1.57- and 2.43-Å resolution, respectively. Structural analysis of the LeIBPs revealed a dimeric right-handed β-helix fold, which is composed of three parts: a large coiled structural domain, a long helix region (residues 96–115 form a long α-helix that packs along one face of the β-helix), and a C-terminal hydrophobic loop region (^{243}PFVPAPEVV^{251}). Unexpectedly, the C-terminal hydrophobic loop region has an extended conformation pointing away from the body of the coiled structural domain and forms intertwined dimer interactions. In addition, structural analysis of glycosylated LeIBP with sugar moieties attached to Asn^{185} provides a basis for interpreting previous biochemical analyses as well as the increased stability and secretion of glycosylated LeIBP. We also determined that the aligned Thr/Ser/Ala residues are critical for ice binding within the B face of LeIBP using site-directed mutagenesis. Although LeIBP has a common β-helical fold similar to that of canonical hyperactive antifreeze proteins, the ice-binding site is more complex and does not have a simple ice-binding motif. In conclusion, we could identify the ice-binding site of LeIBP and discuss differences in the ice-binding modes compared with other known antifreeze proteins and ice-binding proteins.

Antifreeze proteins (AFPs)[3] and ice-binding proteins (IBPs) have been found in many species that live in subfreezing environments. AFPs bind to ice crystals and cause differences between the freezing point and melting point (TH: thermal hysteresis) through an adsorption-inhibition mechanism, thereby protecting organisms from ice damage (1–3). Broadly speaking, IBPs include AFPs and other ice-nucleating proteins. Several IBPs have recently been identified in Antarctic sea ice algae (4–7), yeast (8, 9), fungi (10, 11), mushrooms (12), and bacteria (13, 14). Some of these IBPs can be secreted extracellularly by a cleavable N-terminal signal sequence and may subsequently alleviate cell damage by preventing recrystallization of extracellular ice. Low sequence similarity with other known AFPs suggests that the IBPs may form a new subfamily and have a unique ice-binding mechanism. The IBPs have also been found to exhibit lower levels of TH activity than AFPs, but little is known about the specific ice-binding mechanism of IBPs.

AFPs have been isolated from a variety of organisms and classified into several groups (types I–IV, insect AFPs, bacterial AFPs, and plant AFPs) depending on their structural characteristics and source (15–25). Although each antifreeze class differs dramatically in its sequences and structures and even binds to different planes of ice, the various classes do have some properties in common (2, 3, 26). The ice-binding sites are relatively hydrophobic and flat, which provide good surface-surface complementarity with the ice crystal.

To date, NMR and crystal structures of AFPs from polar fish (15–20), insects (22, 23), and psychrophilic bacteria (21) have been reported. The structures of insect and bacterial AFPs exhibit a β-helical fold, and these proteins have a regular pattern of Thr residues. Two Thr residues are aligned in insect AFPs (Thr-*X*-Thr motif), which may allow the protein to bind to two different basal and prism planes of ice. By contrast, bacterial MpAFP (from *Marinomonas primoryensis*) uses a Thr-*X*-Asx motif located in a flat β-sheet to bind ice. Mutational studies have shown that substitution of this Thr residue with Tyr

* This work was supported by the National Agenda Project from the Korea Research Council of Fundamental Science and Technology (KRCF) and Korea Polar Research Institute (KOPRI) Grant PG11010 and PE11100 (to H. J. K.).

[S] This article contains supplemental Figs. S1 and S2.

The atomic coordinates and structure factors (codes 3UYU and 3UYV) have been deposited in the Protein Data Bank, Research Collaboratory for Structural Bioinformatics, Rutgers University, New Brunswick, NJ (http://www.rcsb.org/).

[1] Both authors contributed equally to this work.

[2] To whom correspondence should be addressed: Division of Polar Life Sciences, Korea Polar Research Institute, Incheon 406-840, Republic of Korea. Tel.: 82-32-260-6253; Fax: 82-32-260-6256; E-mail: hjkim@kopri.re.kr.

[3] The abbreviations used are: AFP, antifreeze protein; IBP, ice-binding protein; r.m.s. deviation, root mean square deviation; TH, thermal hysteresis; LeIBP, *Leucosporidium* IBP; SeMet, selenomethionin.

resulted in a loss of antifreeze activity (27, 28). These data suggest that the Thr residues located in the ice-binding face are involved in ice binding. The β-helical fold provides a conserved ice-binding platform, forming a flat binding surface and common Thr-containing motif.

In previous work, we identified and characterized a moderately active IBP (LeIBP) from Arctic yeast *Leucosporidium* sp. AY30 (8, 9).[4] LeIBP shows a remarkable sequence similarity with IBPs from other fungi, diatoms, or yeast. Comparison of the amino acid sequence of LeIBP to those of other IBPs revealed that LeIBP has 56 and 58% identity to IBPs found in the snow mold *Typhula ishikariensis* (TisIBP) and in the polar diatom *Navicula glaciei* (NglIBP), respectively. Periodic acid-Schiff (PAS) staining and peptide:*N*-glycosidase F treatment further confirmed the glycosylation of secreted LeIBP. Secondary structure prediction and circular dichroism experiments have revealed that IBPs are mainly composed of β-sheet elements similar to other hyperactive β-helical AFPs. However, LeIBP does not contain a simple ice-binding motif as in other hyperactive β-helical AFPs. Moreover, we have shown that LeIBP exhibits distinct differences from other AFPs, including its oligomerization, antifreeze activity, and ice-binding ability (8, 9).[4] It appears to form a dimer in solution based on size exclusion chromatography and analytical ultracentrifugation analysis.[4] The three-dimensional structure of LeIBP is essential for understanding its structure and function. In this study, we describe two crystal structures of non-glycosylated LeIBP produced from *E. coli* and glycosylated LeIBP produced from *Pichia pastoris*. This study presents the first structure of a glycosylated IBP. We compared these structures with other known structures to understand their unusual ice-binding site as well as the role of glycosylation. We present a new class of IBPs with a unique set of ice-binding residues that form a previously undescribed dimer.

EXPERIMENTAL PROCEDURES

Expression, Purification, and Crystallization of LeIBPs—Non-glycosylated LeIBP was expressed in *Escherichia coli*, purified, and crystallized as described previously (9). Selenomethionine (SeMet)-labeled LeIBP (Leu^{86} and Leu^{172} were mutated to methionine because the amino acid sequence of LeIBP contains no methionines) was expressed in *E. coli* B834 cells grown in a minimal medium (M9) supplemented with SeMet and other nutrients and was purified using the same procedure used for the wild-type protein. Briefly, the transformed bacteria were grown at 30 °C in Luria-Bertani (LB) medium containing 50 mg/liter of ampicillin. Bacterial cultures were induced at A_{600} = 0.6 by adding isopropyl 1-thio-β-D-galactopyranoside to 1 mM and incubating at 16 °C for 18 h. After lysis using sonication, the lysate was clarified by centrifugation (12,000 × *g* for 1 h at 4 °C) and loaded onto a nickel-nitrilotriacetic acid-agarose column pre-equilibrated with lysis buffer (20 mM potassium P_i, pH 7.4, 500 mM NaCl, and 5 mM imidazole). The protein was eluted with a 500 mM imidazole gradient. The fractions containing SeMet-labeled LeIBP protein were pooled and dialyzed against lysis buffer. After cleavage of the His_6 tag at 4 °C overnight, the proteins were gel-filtrated on a Superdex 200 column (Amersham Biosciences) equilibrated in a buffer containing 20 mM Tris-HCl, pH 8.0, and 150 mM NaCl. The fractions containing SeMet-labeled LeIBP protein were pooled and concentrated up to 18.2 mg/ml.

TABLE 1
Data collection statistics
Values in parentheses are for the highest-resolution shell.

	Non-glycosylated LeIBPSe-Met peak single-wavelength anomalous dispersion	Glycosylated LeIBP
Data collection		
Space group	$P4_32_12$	$P6_522$
Cell dimensions		
a, *b*, *c* (Å)	97.6, 97.6, 106.6	58.6, 58.6, 292.6
α, β, γ (°)	90.0, 90.0, 90.0	90.0, 90.0, 120.0
Wavelength	0.98227	1.54180
Resolution (Å)	35.99-1.57 (1.66-1.57)	50.78-2.43 (2.56-2.43)
R_{sym}	0.082 (0.317)	0.061 (0.122)
Total data	575,380 (71983)	38,869 (8019)
Unique data	71,520 (10281)	11,149 (1688)
$I/\sigma I$	13.4 (4.6)	14.5 (9.0)
Completeness (%)	99.4 (98.6)	93.8 (99.5)
Redundancy	8.0 (7.0)	3.5 (4.8)

The SeMet-labeled crystals were grown using hanging drop vapor diffusion at 20 °C. The drops consisted of 1 μl of protein solution (18.2 mg/ml in 20 mM Tris-HCl, pH 8.0, and 150 mM NaCl) and 1 μl of reservoir solution (0.1 M sodium acetate, pH 4.5, 1.2 M ammonium sulfate, and 0.2 M NaCl). Cryoprotection was achieved by successive transfer of the crystals into mother liquor supplemented with 10, 15, 20, and 30% glycerol.

Glycosylated LeIBP was expressed in *P. pastoris* and purified as described previously.[4] Briefly, *P. pastoris* transformant cells were grown in 3 liters of YPD medium (1% yeast extract, 1% Bacto-tryptone, and 2% glucose) at 30 °C for 5 days. The culture was supplemented daily with 5 ml of methanol. The culture supernatant was applied to an ion exchange (QFF) column and eluted with a buffer containing 50 mM Tris-HCl, pH 8.0, and 400 mM NaCl. The elution fractions were analyzed by SDS-PAGE and further separated with a Superdex 200 size exclusion column (Amersham Biosciences) equilibrated with a buffer containing 50 mM Tris-HCl, pH 8.0, and 150 mM NaCl at a flow rate of 1 ml/min. The protein was concentrated to ~25 mg/ml prior to the crystallization experiments using a Vivaspin membrane with a molecular mass cutoff of 10 kDa. The protein concentration was determined by measuring the absorbance at 280 nm using a calculated extinction coefficient of 26,930 M^{-1} cm^{-1}. The best crystal used for data collection was grown using the hanging drop vapor diffusion method after mixing with a precipitant solution consisting of 0.1 M imidazole, pH 8.5, 1.7 M potassium phosphate, 0.5 M sodium phosphate, and 0.2 M NaCl using drop ratios of 1 μl of protein to 1 μl of precipitant. Large single crystals grew to a maximum size of 0.5 mm in all directions within 2–3 days.

Data Collection and Structure Determination of LeIBPs—A selenium single-wavelength anomalous dispersion data set was collected to 1.57-Å resolution at the Photon Factory NE3A beam line, and diffraction images were processed and scaled with iMOSFLM (30) and SCALA (31), respectively (Table 1). Four selenium sites were found, and the structure of the SeMet-labeled non-glycosylated LeIBP (21–261) was solved by single-

[4] K. S. Park, J. H. Lee, S. I. Park, H. Do, E. J. Kim, S. H. Kang, and H. J. Kim, unpublished data.

TABLE 2
Refinement statistics
Values in parentheses are for the highest-resolution shell.

	Non-glycosylated LeIBP	Glycosylated LeIBP
Refinement		
Resolution (Å)	31.59-1.57 (1.62-1.57)	50.78-2.43 (2.50-2.43)
No. of reflections of working set	67,692 (4926)	10,549 (788)
No. of reflections of test set	3614 (244)	533 (56)
R-factor	0.216 (0.245)	0.236 (0.340)
R_{free} [a]	0.251 (0.324)	0.286 (0.331)
No. of amino acid residues	480	240
No. of sugar residues	0	4
No. of solvent molecules	458	14
Average *B*-factor (protein) (Å^2)	15.60	23.60
Average *B*-factor (solvent) (Å^2)	31.58	47.81
R.m.s. deviation from ideal geometry		
Covalent bond lengths (Å)	0.026	0.018
Bond angles (°)	2.257	2.208

[a] R_{free} was calculated for a randomly chosen 5% of the reflections.

wavelength anomalous dispersion phasing using the automated search routine AUTOSOL from the PHENIX program suite (32). The initial model was built by AUTOBUILD from PHENIX (32) and was subsequently rebuilt using Coot (33). Refinement of coordinates was then performed using iterative rounds of REFMAC5 refinement (34) and manual rebuilding. The final model contains residues 21–71 and 74–252 from chain A, 21–71 and 74–252 from chain B, and 458 water molecules in the asymmetric unit with 97.8% of residues in the most favored regions of the Ramachandran plot and no residues in the disallowed region (35). The model has r.m.s. deviation values of 0.026 Å for the bond lengths and 2.257 Å for the bond angles. The R_{cryst} and R_{free} values of the final model are 21.6 and 25.1%, respectively (Table 2).

Successful flash freezing was achieved when the glycosylated LeIBP crystals were transferred directly to paratone oil and allowed to equilibrate for 2 min. The native data of glycosylated LeIBP were collected to 2.43-Å resolution at the Korea Basic Science Institute (KBSI) with the x-ray facility home source and processed using iMOSFLM (30) and SCALA (31). The glycosylated LeIBP structure was determined by molecular replacement using the program MOLREP (36). Our refined non-glycosylated LeIBP structure was used as the search model. The entire structure of glycosylated LeIBP was checked and manually rebuilt into the composite omit $2F_{obs} - F_{calc}$ and $F_{obs} - F_{calc}$ electron density maps using Coot (33) with several iterative rounds. Computational refinement was performed using REFMAC5 (34), resulting in a final crystallographic *R* value of 23.6% (R_{free} = 28.6%). The model statistics are shown in Table 2. In the Ramachandran plot, 95.6% of residues are found in the most favored regions, and only one residue is found in the disallowed region (35).

Mutagenesis—Mutations were introduced by site-directed PCR mutagenesis using mutagenic primers. Plasmids for non-glycosylated LeIBP were used as template DNA for mutagenesis. After amplification, the PCR fragments were digested by the DpnI restriction enzyme to eliminate template plasmids. The nucleotide sequences of the desired mutants were confirmed by DNA sequencing. All mutant proteins were expressed from *E. coli* cells and were purified using the same procedure used for the wild-type protein (9, 29).

Antifreeze Activity—Antifreeze (thermal hysteresis) activity was measured using a nanoliter osmometer (Otago Osmometers, Dunedin, New Zealand) connected to a cold well stage mounted on a light microscope and equipped with a Canon digital camera. The sample well was placed on the stage and frozen rapidly by placing the samples on the surface of a cold metal block at approximately −20 °C. The temperature was raised slowly until a single ice crystal remained. The temperature was lowered again slowly, whereas the ice crystal morphology was maintained. The freezing point of the sample was determined to be the temperature at which rapid growth of the ice crystal was observed under the microscope. The maximum difference between the annealing temperature and freezing point during the slow cooling steps was used as an approximation of the freezing point depression activity of the sample. Measurements for the TH activity curve were done in distilled water, and the protein sample concentration ranged from 0 to 500 μM as determined by amino acid analysis.

Model for LeIBP and Ice Crystal Interaction—Docking simulations were performed with HEX 6.3 (40). The structural model for the molecular interaction between LeIBP and ice crystal was built using the computational methods for rigid docking implemented in HEX 6.3 (40). For all of the docking models generated, molecular mechanics energy minimization over the force field implemented in HEX 6.3 (40) was performed. From the overall models, the best complex model in terms of highest steric and electrostatic correlation was selected.

RESULTS

Overall Structure of LeIBP—The structure of non-glycosylated LeIBP (residues 21–261; the first 20 residues, which are a signal sequence, were removed) was determined to a resolution of 1.57 Å by single-wavelength anomalous dispersion from a single SeMet crystal. This structure is the first three-dimensional structure of a fungal, diatom, or yeast IBP. As shown in Fig. 1*A*, two homodimeric molecules were found. The protein forms a dimer in the asymmetric unit in primitive tetragonal space group $P4_32_12$ with cell dimensions a = 97.6 Å, b = 97.6 Å, c = 106.6 Å. The dimer contacts are made through helix α3 and the C-terminal loop (Fig. 1, *A* and *B*, and supplemental Fig. S2*A*). Size exclusion chromatography and cross-linking experiments[4] have shown that LeIBP monomers occur in solution but that the preferred state of the protein is a dimer. The interaction between the α3 helices is mediated through hydrophobic interactions of Val^{30}, Pro^{95}, Tyr^{99}, and Ala^{102}. The C-terminal hydrophobic residues (^{243}PFVPAPEVV^{251}) seem to strengthen the interaction by domain swapping. The loop conformation in the C-terminal region is stabilized by two hydrogen bonds (Val^{251} N-Pro^{58} O and Val^{251} O-Ala^{60} N) and hydrophobic interactions (Pro^{248}, Val^{250}, Ala^{90}, Pro^{97}, and Ala^{101}). However, based on a multiple sequence alignment, the C-terminal tail seems to be missing in other diatom or fungal IBPs. Moreover, the residues involved in the dimer interactions from helix α3 are not well conserved in other IBP sequences, suggesting that dimer formation is a unique feature of LeIBP (Fig. 1*C*).

The monomeric structure of LeIBP has a β-helical fold similar to that of insect and bacterial AFPs. The β-helical folds are stabilized by both intramolecular β-sheet hydrogen bonds and

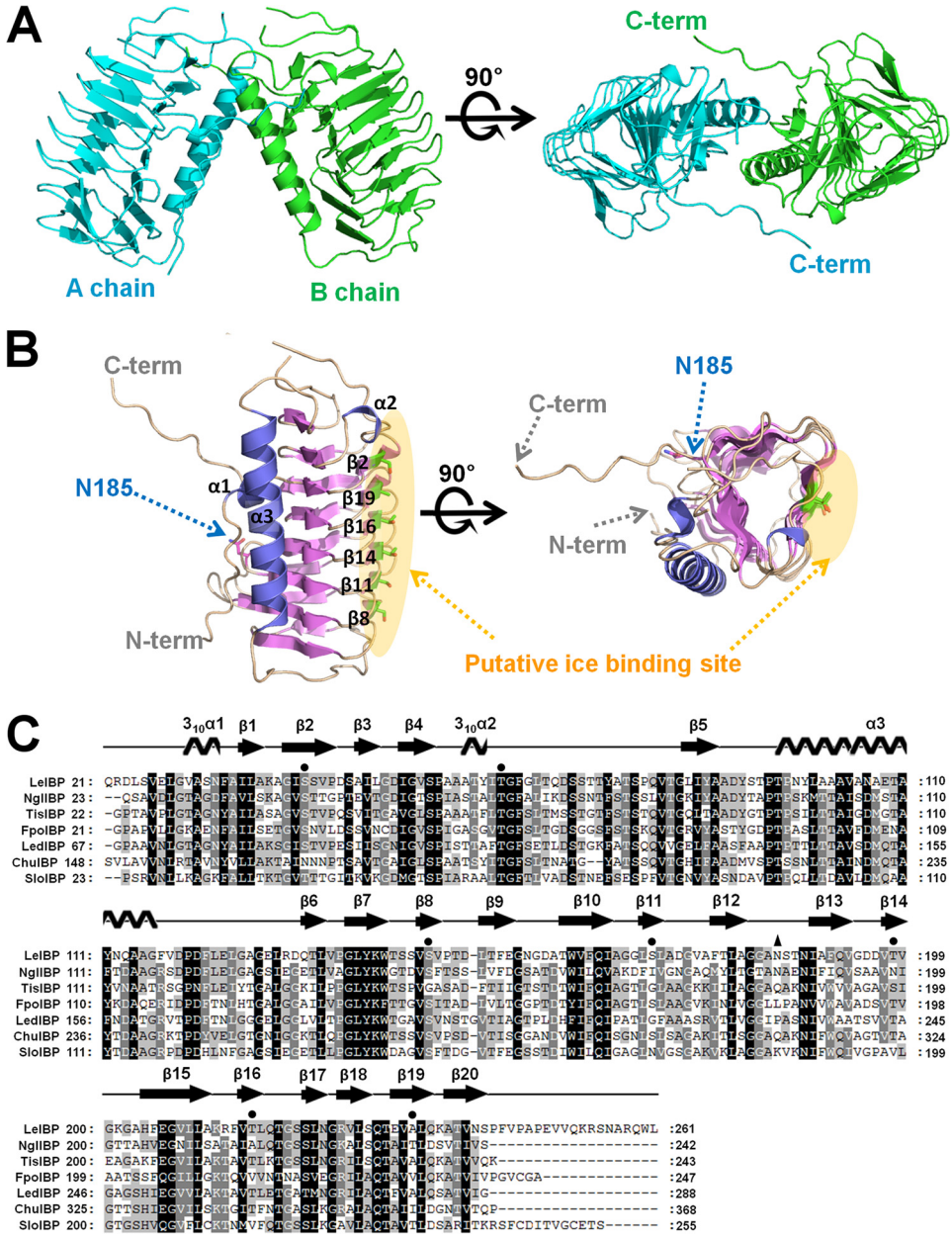

FIGURE 1. **Crystal structure of non-glycosylated LeIBP.** *A,* ribbon diagram of the dimeric structure of LeIBP observed in the asymmetric unit of the crystal. The two subunits are colored *green* and *blue*. *B,* the overall monomeric structure of LeIBP, which adopts a right-handed β-helical fold. *C,* structure-based alignment of the amino acid sequences of IBPs from *Leucosporidium* sp. AY30 (LeIBP), *N. glaciei* (NgIIBP), *T. ishikariensis* (TisIBP), *Flammulina populicola* (FpoIBP), *Lentinula edodes* (LedIBP), *Cytophaga hutchinsonii* ATCC 33406 (ChuIBP), and *Stephos longipes* (SloIBP) using ClustalX (43). Residues constituting the ice-binding sites are indicated by *filled circles*. The glycosylation residue Asn^{185} is marked by a *filled triangle*.

an inner hydrophobic core. Overall, the β-helix is built from three parallel sheets (A, B, and C faces) with dimensions of ~50 Å × 30 Å × 20 Å (Fig. 1). These sides are derived from strands: 1, 4, 5, 7, 10, 13, 15, and 18 (A face); 2, 8, 11, 14, 16 and 19 (B face); and 3, 6, 9, 12, 15, 17, and 20 (C face) (Fig. 1, *A*–*C*). LeIBP shows a number of characteristics distinctive from insect and bacterial AFPs, thereby suggesting that it can be classified into a new IBP family. The most surprising differences were observed in the long helix α3 insertion between β5 and β6, which is formed by residues 96–115 and packs against the core β-helical structure of LeIBP. The amphiphilic nature of helix α3 enables hydrophobic interactions with the A face of the β-helical domain. Residues Tyr^{99}, Leu^{100}, Ala^{103}, Val^{104}, Ala^{107}, Tyr^{111}, and Ala^{110} comprise the hydrophobic face of helix α3. The hydrophobic A face of the β-helix core, which interacts with helix α3, is defined by Leu^{37}, Tyr^{88}, Val^{163}, Ala^{190}, Ala^{208}, Leu^{210}, and Leu^{228}. Moreover, Gln^{113}-NE2 and Asn^{106}-ND2 on the hydrophilic face of helix α3 are further stabilized by intramolecular hydrogen bond interactions with Ser^{25}-O and Leu^{28}-O, respectively, in the N-terminal loop region. Sequence comparison also revealed that an additional α-helix is a common feature for fungal, diatom, and yeast IBPs.

Because sequence alignments indicated that six amino acids (residues ^{137}PGLYKW^{142}) are highly conserved across IBPs from diverse species, we aimed to understand their role in the LeIBP structure. The conserved region forms strand β7, which

is supported by extensive hydrophobic interactions and appears to be a major stabilizing force between helix α3 and the β-helix. In addition, a hydrogen bond between Lys[141] NZ and Gln[165] OE1 further stabilizes the α3–β6 connecting loop conformation. Leu[139] lies between helix α3 and the β-helix core and is stabilized in the hydrophobic pocket formed by Leu[24], Phe[117], Pro[120], and Val[163]. Tyr[140] is flanked with aromatic residues and forms hydrophobic stacking interactions with Phe[122] and Phe[164] within the β-helix core. The side chain of Lys[141] is notably solvent exposed and is positioned to form a hydrogen bond with the side chain of Gln[165]. The side chain of Trp[142] makes hydrophobic contacts with Leu[125], Leu[130], Leu[135], Val[146], Phe[164], and Ile[166]. The highly conserved β7 strand region may play a significant role in the correct folding of LeIBP and intramolecular stabilization may be similar to that in other IBP structures (Fig. 2). We further took an in-depth look at the role of highly conserved residues. Ser[80] located within the α2–β5 connecting loop region is highly conserved and forms a hydrogen bond with the carboxyl group of Phe[67]. This interaction is required for the structural stability of the loop conformation. Additionally, Thr[239] located within the β5 strand is conserved, with the exception of SloIBP, but it is not important for antifreeze function based on our mutagenesis studies.

We also crystallized glycosylated LeIBP and determined its crystal structure at 2.43-Å resolution. Specifically, glycosylated LeIBP was crystallized in hexagonal space group $P6_5$ with cell dimensions $a = 58.6$ Å, $b = 58.6$ Å, $c = 292.6$ Å, $\alpha = 90.0°$, $\beta = 90.0°$, and $\gamma = 120.0°$. One glycosylated LeIBP molecule was observed in the asymmetric unit with a solvent content of 57.7% (V_M = 2.90 Å^3/Da) (Fig. 3*A*). Using a 2-fold crystallographic symmetry axis, this monomer forms a similar dimer structure to that of non-glycosylated LeIBP (r.m.s. deviation of 1.1 Å; over 461 Cα atoms). We believe that the observed dimeric structure of glycosylated LeIBP is physiologically relevant and is supported by earlier work describing the homodimerization of glycosylated LeIBP using analytical size exclusion chromatography. There is one potential *N*-glycosylation site (N-*X*-(S/T)) in the LeIBP sequence at Asn[185]. The crystallographic evidence clearly indicates glycosylation at Asn[185], as previously described.[4] Sufficient electron density was observed for modeling four sugar residues: two NAG (*N*-acetyl-β-D-glucosamine) molecules, one BMA (β-D-mannopyranose), and one MAN (α-D-mannopyranose) (Fig. 3*B*). When the structures of glycosylated LeIBP and non-glycosylated LeIBP structure are superimposed, the overall structures are similar with an r.m.s. deviation of 0.3 Å over 231 Cα atoms; however, the side chain of Phe[244] shows a rotational movement (about 80°) toward the bound glycans (Fig. 3*C*). The glycan molecules of glycosylated LeIBP form direct hydrophobic interactions with Phe[244] and Pro[246] and hydrogen bonds with NAG O5 and Thr[187] OG1; moreover, water-mediated hydrogen bonds are formed with NAG O3, BMA O5, and MAN O5. *N*-Linked glycosylation of LeIBP expressed in *P. pastoris* was previously confirmed by SDS-PAGE and periodic acid-Schiff staining.[4] The native LeIBP produced from *Leucosporidium* sp. also contains a glycoside chain. The glycosylation site is exposed to the solvent region and is located at the interface between the two protomers but far from the putative active site. These results demonstrate that *N*-linked glycosylation is not required for LeIBP activity, in accordance with previous observations in antifreeze activity experiments.[4] Although the glycosylated LeIBP expressed in *P. pastoris* shows antifreeze activity similar to the bacterially expressed recombinant protein non-glycosylated LeIBP,[4] the two proteins show different stabilities. In our cross-linking experiments, non-glycosylated LeIBP was more easily oligomerized than glycosylated LeIBP into aggregates. Glycosylation-free mutants (N185Q and N185A) seemed to be retained

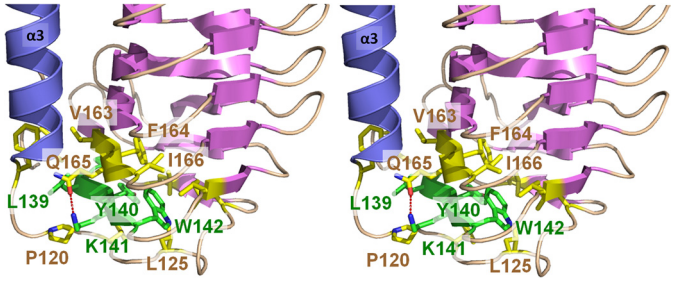

FIGURE 2. **The stereo diagram shows an interaction network around highly conserved residues (**^{137}**PGLYKW**^{142}**) in strand β7 (*green color*).** Hydrogen bonding between Lys[141] and Gln[165] and several hydrophobic interactions stabilize strand β7 and the connecting loop.

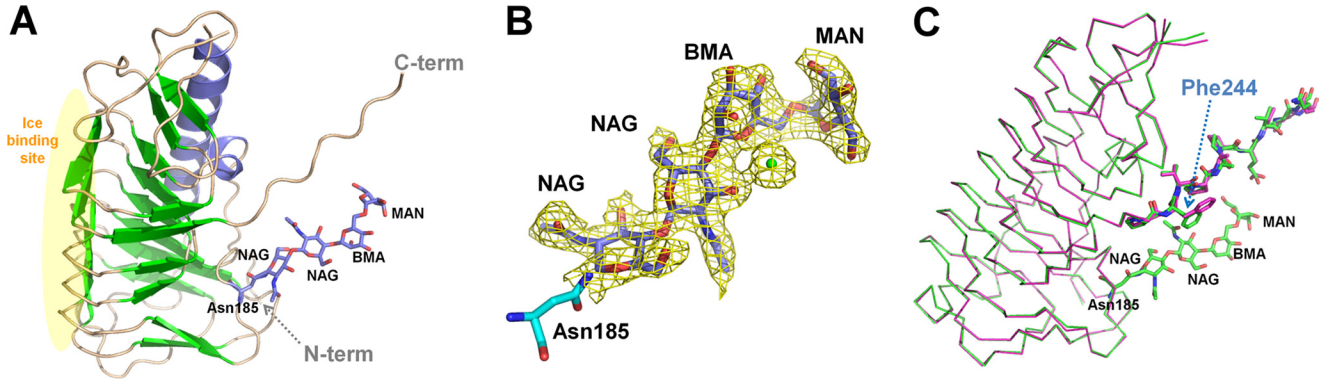

FIGURE 3. **Overall structure of glycosylated LeIBP.** *A*, glycosylation at Asn[185] is shown with the stick model. The modeled *N*-glycans contain two *N*-acetyl-β-D-glucosamine (*NAG*) molecules, one β-D-mannopyranose (*BMA*), and one α-D-mannopyranose (*MAN*). The four sugar residues at Asn[185] were unambiguously positioned in the electron density map. *B*, $2F_o - F_c$ electron density map at the 1σ contour level around Asn[185]. The four sugar residues and a water molecule are shown in the *stick model and sphere*, respectively. *C*, superposition of non-glycosylated LeIBP and glycosylated LeIBP. Glycosylated LeIBP is shown in *slate green* and non-glycosylated LeIBP is depicted in *magenta*. Phe[244] adopts a different conformation in the glycosylated LeIBP structure. All figures were prepared using the program PyMOL (29).

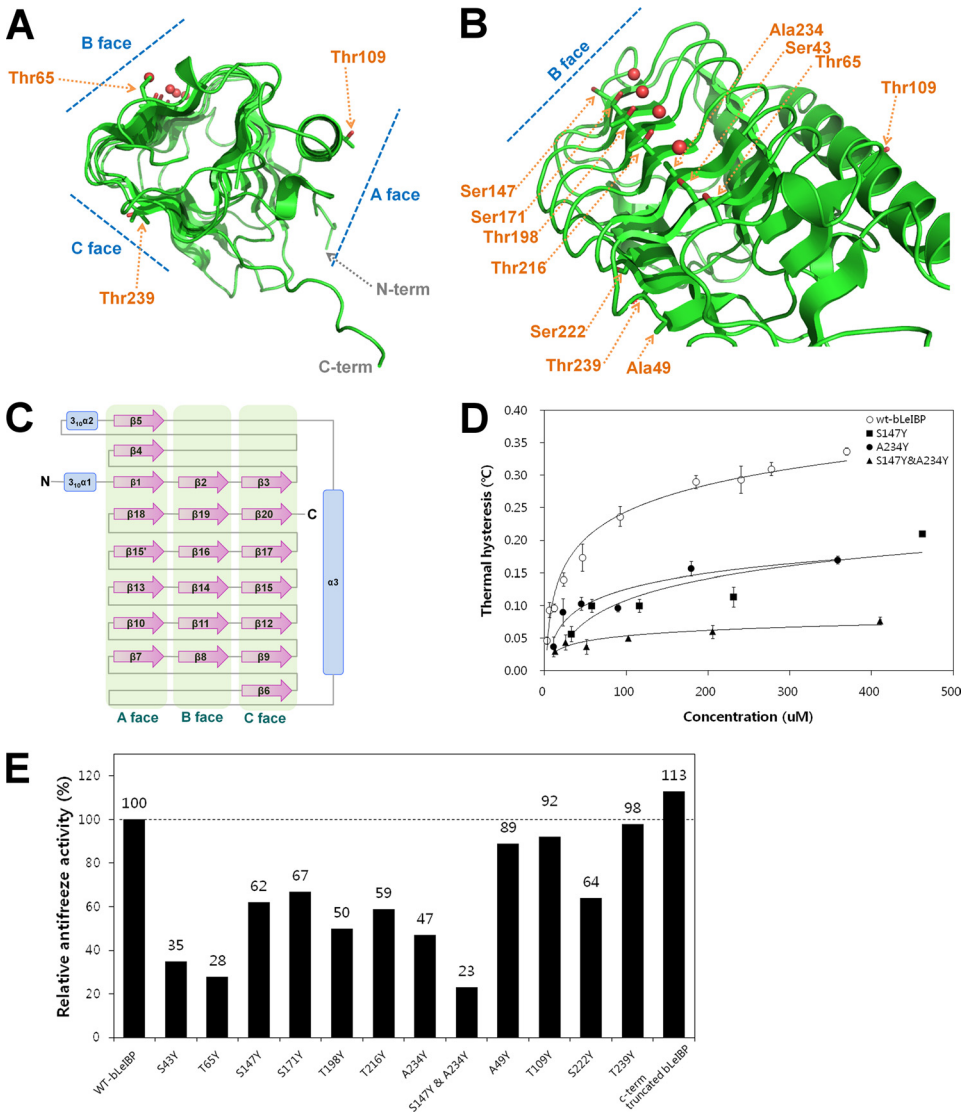

FIGURE 4. **Summary of mutation effects on LeIBP.** *A,* the location of each mutation on the trigonal cylinder structure is shown in the stick model. Ordered water molecules (*red spheres*) are presented on the B face beside the aligned Thr/Ser/Ala residues. *B,* amino acid side chains mutated in these studies are labeled. The mutant proteins were purified to near homogeneity and were compared with wild-type non-glycosylated LeIBP for their antifreeze activities. *C,* topology diagram of LeIBP structure. α-Helices and β-strands are shown as *cylinders* and *arrows*, respectively. *D*, the TH activities of wild-type and mutant non-glycosylated LeIBP are plotted as a function of concentration. *E,* comparisons of the antifreeze activities of the wild-type non-glycosylated LeIBP and the mutants at 370 μM concentration.

in the cells (data not shown here), suggesting that glycosylation may contribute to LeIBP folding and secretion.

Structural Homology Search—A structural homology search using the program DALI revealed that the best score (Z value of 7.4) was produced by *Haemophilus influenzae* HMW1 Pro-piece, a structural domain essential for bacterial two-partner secretion (Protein Data Bank code 2ODL) (37). This protein shares 9% sequence identity to LeIBP and can be superimposed with an r.m.s. deviation of 3.1 Å for 113 Cα pairs. The right-handed β-helical structure of HMW1 Pro-piece consists of 47 β-strands and 2 α-helices. By contrast, the LeIBP structure is formed by 20 β-strands and one α-helix. In addition to other hemolysins, another bacterial antifreeze protein MpAFP structure (21) with a low score was identified in the homology search. To the best of our knowledge, the topology of the LeIBP structure has not been previously observed. Its two β-helical domains are separated by a long helix insertion, which is distinct from previously reported proteins within the family of all-β-helical AFP structures.

Ice-binding Site of LeIBP—Structural data have revealed that different types of AFPs (types I–IV, fish AFPs, insect AFPs, and plant AFPs) have completely different folds but share common ice-binding sites, which are relatively flat and hydrophobic. The LeIBP structure presented herein adopts an overall β-helical fold similar to that of hyperactive AFPs. To relate the structural information of LeIBP with its ice-binding and functional properties, we targeted the putative ice-binding site of LeIBP by site-directed mutagenesis. The main objective of these experiments was to search for mutations with differential effects on ice binding. The mutants were characterized by their antifreeze and recrystallization inhibition activities. We initially focused on Ser^{43}, Thr^{65}, Ser^{147}, Ser^{171}, Thr^{198}, Thr^{216}, and Ala^{234}, which are located on the B face of the LeIBP structure (Fig. 4, *A–C*). The S147Y and A234Y mutations reduced the antifreeze activ-

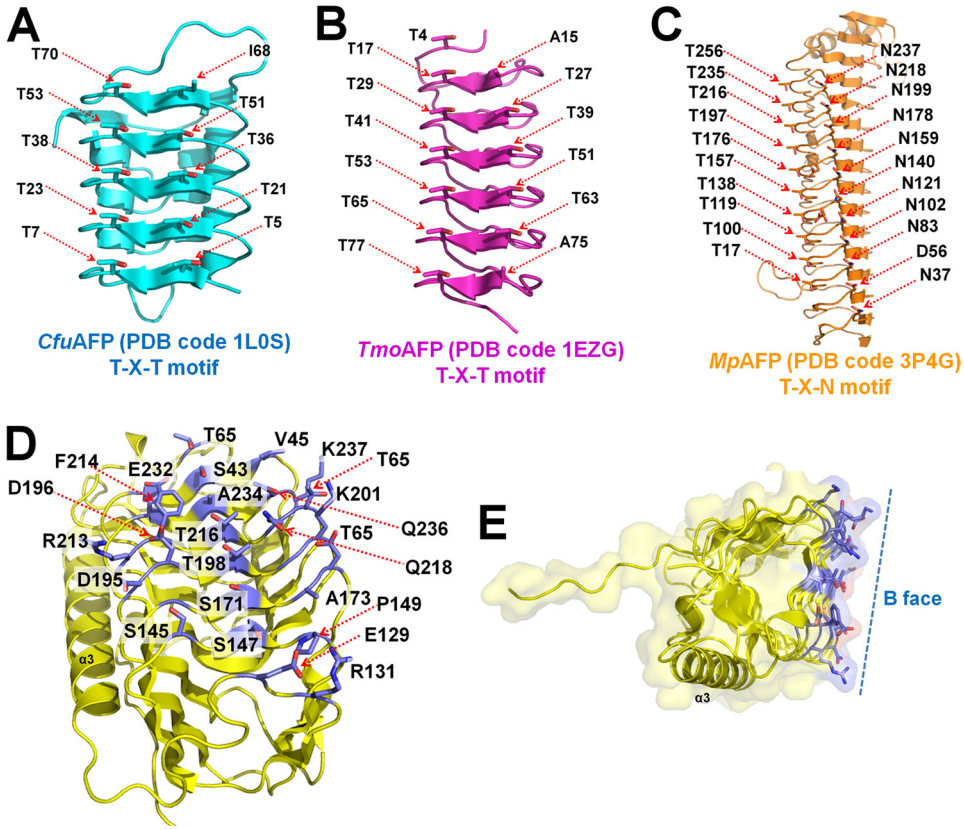

FIGURE 5. **Comparison of ice-binding motifs of β-helical AFPs and LeIBP.** *A*, the T*X*T ice binding motif (where *X* represents any amino acid) of the left-handed β-helical CfuAFP from spruce budworm (*Choristoneura fumiferana*). *B*, the T*X*T ice binding motif of right-handed β-helical TmoAFP from beetle (*Tenebrio molitor*). *C*, the T*X*N ice binding motif of right-handed β-helical MpAFP from an Antarctic bacterium (*M. primoryensis*). *D*, the ice-binding site of right-handed β-helical LeIBP. The ice-binding site residues of LeIBP are more complex and diverse compared with other β-helical AFP structures. *E*, the LeIBP structure presents a flat ice-binding site (B face), which was confirmed in site-directed mutagenesis studies.

ity of non-glycosylated LeIBP (62 and 47% activity of wild type at 370 μM, respectively). Mutation of Thr to Tyr, which confers steric hindrance to ice binding, caused a large reduction in antifreeze activity (38). Furthermore, double mutation of S147Y/A234Y abolished most of the antifreeze activity, suggesting that the B face is the ice-binding face of LeIBP (Fig. 4*D*). By contrast, residues on the other faces (Ala^{49}, Thr^{109}, Ser^{222}, and Thr^{239}) are not involved in ice binding (Fig. 4*E*). Therefore, we propose that the putative ice-binding site contains a regular pattern of aligned Thr, Ser, and Ala residues on the B face of LeIBP. Notably, the C-terminal truncated LeIBP (residues 21–243) showed 13% higher antifreeze activity than the wild-type protein at 370 μM but exhibited a loss of dimer interactions according to our analytical size exclusion chromatography experiment (data not shown). As a result, the ice-binding site would be freely accessible for ice binding in the monomeric state, which may confer higher TH activity to the C-terminal truncated mutant. Additionally, circular dichroism studies showed that the secondary structure of all mutants was similar to that of wild-type LeIBP. These results suggest that the overall conformation of the mutants was unaffected by mutagenesis (supplemental Fig. S1).

Before the structural studies, it was difficult to predict the ice-binding sites of LeIBP based on sequence alignment because of the lack of an ice-binding consensus sequence, such as T*X*T or T*X*N, which is present in hyperactive β-helical AFPs (21–23, 39). Thus, the ice-binding site of LeIBP was believed to be distinct from those of canonical hyperactive β-helical AFPs and was confirmed by the mutagenesis experiments. The hyperactive β-helical AFPs are well known for having specific ice crystal plane preferences; moreover, each ice-binding motif, such as T*X*T or T*X*N, interacts with basal or prism planes of the ice crystal lattice. Comparisons between the new structure and previously determined hyperactive AFP structures revealed that the ice-binding site residues of LeIBP are more complex and diverse. LeIBP does not have a simple ice-binding motif compared with CfuAFP (Fig. 5*A*) (22, 23), TmoAFP (T*X*T motif) (Fig. 5*B*) (39), and MpAFP (T*X*N motif) (21) (Fig. 5*C*). This complex binding mode could explain the broad binding of LeIBP to both basal and prism planes of ice crystal lattices. Indeed, previous work indicated that LeIBP has loose selectivity and can bind to basal planes as well as prism planes.[4] Thus, our findings suggest that LeIBP serves as a broad ice-binding site for ice crystal interactions with more than one strict ice-binding motif arrangement. Furthermore, side chains can reorient when they bind to ice crystals, providing further possibilities for diverse modes of ice crystal recognition.

Next, we used the results of the mutagenesis experiments to build an ice-binding model for the putative interaction between LeIBP and ice crystals *in silico* using the rigid docking module in the program HEX (40). The basal plane of an ice crystal was selected for initial positioning based on results of an ice-etching experiment.[4] We selected the model with the highest score in

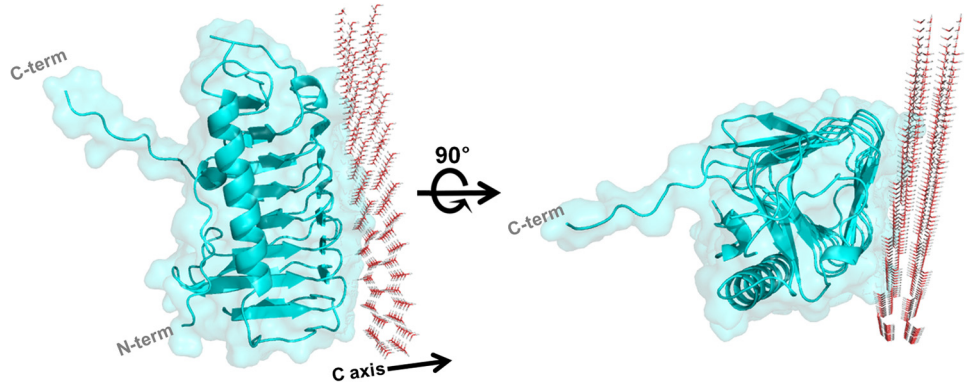

FIGURE 6. **Docking simulations were performed with HEX 6.3 (40).** The structural model for the molecular interaction between LeIBP and basal plane of ice crystal was built using the computational methods for rigid docking implemented in the program HEX (40).

terms of steric and electrostatic correlations, and we applied energy minimization steps to correct unrealistic contacts. The final model for the interaction between LeIBP and ice crystal is shown in Fig. 6. Remarkably, the B face of LeIBP showed high surface complementarity to the surface of the basal plane of the ice crystal without a significant conformational change upon binding (supplemental Fig. S2*B*). These results suggest that ice binding of LeIBP does not require any major conformational change. The hydrophobic effect seems to be a dominant driving force in the interaction between LeIBP and the ice crystal because significant hydrophobic patches are located in complementary positions on the interaction surfaces (Fig. 5, *D* and *E*).

DISCUSSION

We previously identified and characterized the novel ice-binding protein LeIBP from Arctic yeast that effectively inhibits growth of ice crystals (8, 29). In this study, we extended this work by examining the LeIBP structure, revealing the architecture of the ice-binding site, which is essential for mediating the ice crystal interaction. This work presents the first structure of an ice-binding protein from a psychrophilic fungal, diatom, or yeast IBP. Despite the species diversity among members of the IBP family, analysis of the LeIBP structure suggests that IBPs have a common structural domain required for ice binding and adopt right-handed β-helical structures. Considering their overall sequence similarities, the LeIBP structure can likely serve as a structural model for a large number of IBPs.

The crystal structure presented in this study shows the molecular details of LeIBP, including the dimer interface, the different structure of the β-helical domain, and the novel ice-binding site. Our structural and functional analysis of LeIBP provided several surprising results. First, as previously shown, the protein is a dimer in solution with a molecular mass of 45,000–53,000 Da (29). In addition, LeIBP seems to dimerize via the hydrophobic surfaces of helix α3 and the C-terminal loop region to conceal the hydrophobic areas from the solvent. AFPs are typically monomeric, and the only other two documented examples of dimeric AFPs are a type II AFP from rainbow smelt (41) and a hyperactive type I AFP (42). Thus, our results are the first report of an IBP with novel dimeric interactions and a β-helical fold. Second, the crystal structure of LeIBP displays a β-helical structure separated by an α-helix insertion, which is an unprecedented architecture. Importantly, LeIBP has a long helix between strands 4 and 5, rather than the β-helical structure commonly found in other insect and bacterial AFP structures. Third, the ice-binding site of LeIBP is distinct from other previously reported AFPs and IBPs. Notably, the ice-binding site residues of LeIBP are not strictly conserved in IBPs of other species, indicating that the side chains of the ice-binding site do not provide many interactions for ice binding. Instead, proper surface-surface complementary may be particularly important for ice binding. We speculate that the unique and complex ice-binding site allows for interactions with multiple faces of the ice crystal.

Previous work has demonstrated that non-glycosylated LeIBP exhibits ~30% antifreeze activity compared with native LeIBP.[4] We initially suspected that these different activities were due to *N*-glycosylation, which can only occur at Asn^{185}. However, the antifreeze activity of native LeIBP was not significantly affected by deglycosylation, indicating that other factors may affect glycosylated LeIBP activation. In a previous report,[4] we demonstrated that unknown impurities enhanced the antifreeze activity of LeIBP. In addition, Bayer-Giraldi *et al.* (4) recently showed that the TH activity of an AFP from a polar diatom (*Fragilariopsis cylindrus*) was increased by addition of salt. Secretion of enhancers such as salt or polysaccharides, which accumulate in the brine channel in ice, may help to preserve the liquid environment. Since Arctic yeast *Leucosporidium* sp. AY30 secretes LeIBPs, the LeIBP may protect the cell membrane extracellularly and play a role in suppressing the growth of ice crystals in brine pockets. Moreover, the increased antifreeze activity of LeIBP by enhancers appears to be essential for the survival of psychrophilic yeast at low temperatures. However, several questions regarding how the molecules are secreted and whether the LeIBP is secreted in the monomeric or dimeric state remain to be answered. Furthermore, it remains to be established whether the dimer structure enhances activity or whether monomers also bind to ice.

Acknowledgments—We thank Hye Eun Song for help in protein production and crystallization. We also thank the staff at beamline NE3A of the Photon Factory (Tsukuba, Japan) and the x-ray core facility of Korea Basic Science Institute (KBSI) (Ochang, Korea).

REFERENCES

1. D'Amico, S., Collins, T., Marx, J. C., Feller, G., and Gerday, C. (2006) Psychrophilic microorganisms. Challenges for life. *EMBO Rep.* **7,** 385–389
2. Davies, P. L., Baardsnes, J., Kuiper, M. J., and Walker, V. K. (2002) Structure and function of antifreeze proteins. *Philos. Trans. R. Soc. Lond. B Biol. Sci.* **357,** 927–935
3. Venketesh, S., and Dayananda, C. (2008) Properties, potentials, and prospects of antifreeze proteins. *Crit. Rev. Biotechnol.* **28,** 57–82
4. Bayer-Giraldi, M., Weikusat, I., Besir, H., and Dieckmann, G. (2011) Characterization of an antifreeze protein from the polar diatom *Fragilariopsis cylindrus* and its relevance in sea ice. *Cryobiology* **63,** 210–219
5. Janech, M., Krell, A., Mock, T., Kang, J. S., and Raymond, J. A. (2006) Ice-binding proteins from sea ice diatoms (bacillariophyceae). *J. Phycol.* **42,** 410–416
6. Krell, A., Beszteri, B., Dieckmann, G., Glöcknerb, G., Valentina, K., and Mockac, T. (2008) A new class of ice-binding proteins discovered in a salt-stress-induced cDNA library of the psychrophilic diatom *Fragilariopsis cylindrus* (Bacillariophyceae). *Eur. J. Phycol.* **43,** 423–433
7. Raymond, J. A., Janech, M., and Fritsen, C. (2009) Novel ice-binding proteins from a psychrophilic antarctic alga (Chlamydomonadaceae, Chlorophyceae). *J. Phycol.* **45,** 130–136
8. Lee, J. K., Park, K. S., Park, S., Park, H., Song, Y. H., Kang, S. H., and Kim, H. J. (2010) An extracellular ice-binding glycoprotein from an Arctic psychrophilic yeast. *Cryobiology* **60,** 222–228
9. Park, A. K., Park, K. S., Kim, H. J., Park, H., Ahn, I. Y., Chi, Y. M., and Moon, J. H. (2011) Crystallization and preliminary x-ray crystallographic studies of the ice-binding protein from the Antarctic yeast *Leucosporidium* sp. AY30. *Acta Cryststallogr. Sect. F Struct. Biol. Crystallogr.* **67**, 800–802
10. Hoshino, T., Kiriaki, M., Ohgiya, S., Fujiwara, M., Kondo, H., Nishimiya, Y., Yumoto, I., and Tsuda, S. (2003) Antifreeze proteins from snow mold fungi. *Can. J. Bot.* **81,** 1175–1181
11. Xiao, N., Suzuki, K., Nishimiya, Y., Kondo, H., Miura, A., Tsuda, S., and Hoshino, T. (2010) Comparison of functional properties of two fungal antifreeze proteins from *Antarctomyces psychrotrophicus* and *Typhula ishikariensis*. *FEBS J.* **277,** 394–403
12. Raymond, J. A., and Janech, M. G. (2009) Ice-binding proteins from enoki and shiitake mushrooms. *Cryobiology* **58,** 151–156
13. Raymond, J. A., Christner, B. C., and Schuster, S. C. (2008) A bacterial ice-binding protein from the Vostok ice core. *Extremophiles* **12,** 713–717
14. Raymond, J. A., Fritsen, C., and Shen, K. (2007) An ice-binding protein from an Antarctic sea ice bacterium. *FEMS Microbiol. Ecol.* **61,** 214–221
15. Antson, A. A., Smith, D. J., Roper, D. I., Lewis, S., Caves, L. S., Verma, C. S., Buckley, S. L., Lillford, P. J., and Hubbard, R. E. (2001) Understanding the mechanism of ice binding by type III antifreeze proteins. *J. Mol. Biol.* **305,** 875–889
16. Kwan, A. H., Fairley, K., Anderberg, P. I., Liew, C. W., Harding, M. M., and Mackay, J. P. (2005) Solution structure of a recombinant type I sculpin antifreeze protein. *Biochemistry* **44,** 1980–1988
17. Liu, Y., Li, Z., Lin, Q., Kosinski, J., Seetharaman, J., Bujnicki, J. M., Sivaraman, J., and Hew, C. L. (2007) Structure and evolutionary origin of Ca^{2+}-dependent herring type II antifreeze protein. *PLoS One* **2,** e548
18. Nishimiya, Y., Kondo, H., Takamichi, M., Sugimoto, H., Suzuki, M., Miura, A., and Tsuda, S. (2008) Crystal structure and mutational analysis of Ca^{2+}-independent type II antifreeze protein from longsnout poacher, *Brachyopsis rostratus*. *J. Mol. Biol.* **382,** 734–746
19. Patel, S. N., and Graether, S. P. (2010) Structures and ice-binding faces of the alanine-rich type I antifreeze proteins. *Biochem. Cell Biol.* **88,** 223–229
20. Siemer, A. B., and McDermott, A. E. (2008) Solid-state NMR on a type III antifreeze protein in the presence of ice. *J. Am. Chem. Soc.* **130,** 17394–17399
21. Garnham, C. P., Campbell, R. L., and Davies, P. L. (2011) Anchored clathrate waters bind antifreeze proteins to ice. *Proc. Natl. Acad. Sci. U.S.A.* **108,** 7363–7367
22. Graether, S. P., Kuiper, M. J., Gagné, S. M., Walker, V. K., Jia, Z., Sykes, B. D., and Davies, P. L. (2000) β-Helix structure and ice-binding properties of a hyperactive antifreeze protein from an insect. *Nature* **406,** 325–328
23. Leinala, E. K., Davies, P. L., and Jia, Z. (2002) Crystal structure of β-helical antifreeze protein points to a general ice binding model. *Structure* **10,** 619–627
24. Middleton, A. J., Brown, A. M., Davies, P. L., and Walker, V. K. (2009) Identification of the ice-binding face of a plant antifreeze protein. *FEBS Lett.* **583,** 815–819
25. Smallwood, M., Worrall, D., Byass, L., Elias, L., Ashford, D., Doucet, C. J., Holt, C., Telford, J., Lillford, P., and Bowles, D. J. (1999) Isolation and characterization of a novel antifreeze protein from carrot (*Daucus carota*). *Biochem. J.* **340,** 385–391
26. Jia, Z., and Davies, P. L. (2002) Antifreeze proteins. An unusual receptor-ligand interaction. *Trends Biochem. Sci.* **27,** 101–106
27. Doucet, D., Tyshenko, M. G., Kuiper, M. J., Graether, S. P., Sykes, B. D., Daugulis, A. J., Davies, P. L., and Walker, V. K. (2000) Structure-function relationships in spruce budworm antifreeze protein revealed by isoform diversity. *Eur. J. Biochem.* **267,** 6082–6088
28. Graether, S. P., and Sykes, B. D. (2004) Cold survival in freeze-intolerant insects. The structure and function of β-helical antifreeze proteins. *Eur. J. Biochem.* **271,** 3285–3296
29. DeLano, W. L. (2004) *The PyMOL Molecular Graphics System*, DeLano Scientific LLC, San Carlos, CA
30. Leslie, A. G. (2006) The integration of macromolecular diffraction data. *Acta Crystallogr. D Biol. Crystallogr.* **62,** 48–57
31. Collaborative Computational Project, Number 4 (1994) The CCP4 suite. Programs for protein crystallography. *Acta Crystallogr. D Biol. Crystallogr.* **50,** 760–763
32. Adams, P. D., Gopal, K., Grosse-Kunstleve, R. W., Hung, L. W., Ioerger, T. R., McCoy, A. J., Moriarty, N. W., Pai, R. K., Read, R. J., Romo, T. D., Sacchettini, J. C., Sauter, N. K., Storoni, L. C., and Terwilliger, T. C. (2004) Recent developments in the PHENIX software for automated crystallographic structure determination. *J. Synchrotron. Radiat.* **11,** 53–55
33. Emsley, P., and Cowtan, K. (2004) Coot. Model-building tools for molecular graphics. *Acta Crystallogr. D* **60,** 2126–2132
34. Murshudov, G. N., Vagin, A. A., and Dodson, E. J. (1997) Refinement of macromolecular structures by the maximum-likelihood method. *Acta Crystallogr. D* **53,** 240–255
35. Davis, I. W., Leaver-Fay, A., Chen, V. B., Block, J. N., Kapral, G. J., Wang, X., Murray, L. W., Arendall, W. B., 3rd, Snoeyink, J., Richardson, J. S., and Richardson, D. C. (2007) MolProbity. All-atom contacts and structure validation for proteins and nucleic acids. *Nucleic Acids Res.* **35,** W375–383
36. Vagin, A., and Teplyakov, A. (1997) *MOLREP*: an automated program for molecular replacement. *J. Appl. Crystallogr.* **30,** 1022–1025
37. Yeo, H. J., Yokoyama, T., Walkiewicz, K., Kim, Y., Grass, S., and Geme, J. W., 3rd (2007) The structure of the *Haemophilus influenzae* HMW1 pro-piece reveals a structural domain essential for bacterial two-partner secretion. *J. Biol. Chem.* **282,** 31076–31084
38. Garnham, C. P., Gilbert, J. A., Hartman, C. P., Campbell, R. L., Laybourn-Parry, J., and Davies, P. L. (2008) A Ca^{2+}-dependent bacterial antifreeze protein domain has a novel β-helical ice-binding fold. *Biochem. J.* **411,** 171–180
39. Liou, Y. C., Tocilj, A., Davies, P. L., and Jia, Z. (2000) Mimicry of ice structure by surface hydroxyls and water of a β-helix antifreeze protein. *Nature* **406,** 322–324
40. Ritchie, D. W., and Kemp, G. J. (2000) Protein docking using spherical polar Fourier correlations. *Proteins* **39,** 178–194
41. Achenbach, J. C., and Ewart, K. V. (2002) Structural and functional characterization of a C-type lectin-like antifreeze protein from rainbow smelt (*Osmerus mordax*). *Eur. J. Biochem.* **269,** 1219–1226
42. Marshall, C. B., Chakrabartty, A., and Davies, P. L. (2005) Hyperactive antifreeze protein from winter flounder is a very long rod-like dimer of α-helices. *J. Biol. Chem.* **280,** 17920–17929
43. Thompson, J. D., Gibson, T. J., Plewniak, F., Jeanmougin, F., and Higgins, D. G. (1997) The CLUSTAL_X windows interface. Flexible strategies for multiple sequence alignment aided by quality analysis tools. *Nucleic Acids Res.* **25,** 4876–4882